East Eur. J. Phys. **3**. 5-10 (2020) DOI:10.26565/2312-4334-2020-3-01

PACS: 61.50.Lt, 61.72.Ff, 62.23.Pq, 68.35 Fx, 68.35.Np, 81.05.Je, 81.40.Cd

STRUCTURE AND CORROSION OF QUASICRYSTALLINE CAST Al–Co–Ni AND Al–Fe–Ni ALLOYS IN AQUEOUS NaCl SOLUTION

Olena V. Sukhova*, Volodymyr A. Polonskyy
Oles Honchar Dnipro National University
72, Haharin Ave., Dnipro, 49010, Ukraine
**Corresponding Author: sukhovaya@ukr.net*
Received March 23, 2020; revised April 6, 2020; accepted May 30, 2020

In this work the structure and corrosion behavior of quasicrystalline cast $Al_{69}Co_{21}Ni_{10}$ and $Al_{72}Fe_{15}Ni_{13}$ alloys in 5-% sodium chloride solution (pH 6.9–7.1) were investigated. The alloys were cooled at 5 K/s. The structure of the samples was studied by methods of quantitative metallography, X-ray analysis, and scanning electron microscopy. Corrosion properties were determined by potentiodynamic method. Stationary potential values were measured by means of long-term registration of (E,τ)–curves using ПИ-50-1 potentiostat and ПР–8 programmer with three-electrode electrolytic cell. A platinum electrode served as counter electrode and silver chloride – as reference electrode. The made investigations confirm the formation of stable quasicrystalline decagonal D-phase in the structure of $Al_{69}Co_{21}Ni_{10}$ and $Al_{72}Fe_{15}Ni_{13}$ alloys. In $Al_{69}Co_{21}Ni_{10}$ alloy, at room temperature D-phase coexists with crystalline $Al_9(Co,Ni)_2$ phase, and in $Al_{72}Fe_{15}Ni_{13}$ alloy – with Al_5FeNi phase. Comparison of Vickers hardness of these phases exhibits the following sequence: H(D-AlCoNi)>H(D-AlFeNi)>H(Al_5FeNi)>H($Al_9(Co,Ni)_2$). In 5 % sodium chloride solution, the investigated alloys corrode under electrochemical mechanisms with oxygen depolarization. Compared with $Al_{72}Fe_{15}Ni_{13}$ alloy, $Al_{69}Co_{21}Ni_{10}$ alloy has less negative value of stationary potential (–0,48 V and –0,40 V, respectively), and its electrochemical passivity region extends due to the inhibition of anodic processes. For both alloys, transition to passive state in the saline solution is observed. A corrosion current density, calculated from (E,lgi)-curve, for $Al_{69}Co_{21}Ni_{10}$ alloy amounts to 0.12 mA/cm^2 and for $Al_{72}Fe_{15}Ni_{13}$ alloy – to 0.14 mA/cm^2. After immersion in the saline solution for 8 days, pits are revealed on the surface of the alloys in areas, mainly where the phase boundaries and flaws are located. The number and size of pits are smaller on the surface of $Al_{69}Co_{21}Ni_{10}$ alloy as compared with those on the surface of $Al_{72}Fe_{15}Ni_{13}$ alloy. The lower corrosion resistance of $Al_{72}Fe_{15}Ni_{13}$ alloy may be explained by the presence of iron-containing phases in its structure. Based on obtained results, the $Al_{69}Co_{21}Ni_{10}$ alloy has been recommended as coating material for rocket-and-space equipment working in marine climate.
KEYWORDS: decagonal quasicrystals, structure, Vickers hardness, electrochemical polarization, pitting corrosion.

The ternary Al–Co–Ni and Al–Fe–Ni alloys are the most interesting stable quasicrystalline materials having decagonal rotation symmetry [1-8]. Decagonal quasicrystals combine two different types of order, periodicity along the rotational axis and non-periodic order perpendicular to it. This property sets decagonal phases apart from periodic crystals, as well as from icosahedral quasicrystals. The interest also is prompted due to the finding of quasicrystalline phases of the above alloys when they are cast under conventional solidification techniques. Quasicrystals have many attractive properties, such as high hardness, low electrical and thermal conductivities, low surface energy, accompanied by a low coefficient of friction, reasonable oxidation and strong corrosion resistance, and unusual optical properties which have not been observed for crystalline alloys [9-13]. These properties can only be used for technological applications in the form of thin film coatings [14-18] or reinforcement particles in metal matrix composites [19-23] in order to circumvent their intrinsic brittleness. In the course of their operation, Al–Co–Ni and Al–Fe–Ni alloys are often subjected to the action of corrosive media, but very little information is available on how such alloys behave in corrosion media.

For many applications of quasicrystalline coatings, e.g. for equipment of mobile platforms for equatorial launches of loads on specialized Zenit-3SL rockets, corrosion resistance under conditions of marine climate is of utmost importance. Therefore, aim of this paper is to investigate structure of quasicrystalline and crystalline phases observed in the cast Al–Co–Ni and Al–Fe–Ni alloys and compare their corrosion characteristics in aqueous sodium chloride solution.

MATERIALS AND METHODS

The quasicrystalline $Al_{69}Co_{21}Ni_{10}$ and $Al_{72}Fe_{15}Ni_{13}$ alloys were prepared by melting of chemically pure components (<99.99 wt. pct.) in a graphite crucible in a Tamman furnace. The samples were cooled at a rate of 5 K/s. The compositions of the alloys were set close to the compositional range where the decagonal phase had been firstly obtained [2,7]. The average chemical composition of the alloys was studied by atomic absorption spectroscopy method. The relative precision of the measurements was better than ± 1 at. pct. The alloys were examined by *Neophot* light-optical microscope (OM). Quantitative metallography was carried out with structural analyzer *Epiquant*. X-ray diffraction analysis (XRD) was done to identify the existing phases in produced samples on an X-ray diffractometer *ДРОН-УМ* with CuK_α source. The local phase compositions were determined in a scanning electron microscope *РЭММА 102-02* by energy-dispersive spectroscopy (EDS) on polished unetched cross-sections.

Corrosion behavior was investigated in 5-% NaCl aqueous solution (pH 6.9–7.1) at the temperature of 293±2 K. Electrochemical measurements were performed using a computer-controlled system including *ПИ-50-1* potentiostat and *ПР-8* programmer using three-electrode electrolytic cell. The investigated sample was used as working electrode, a

platinum plate – as counter electrode, and silver chloride electrode – as reference electrode. A surface of 1 cm^2 was exposed to the solution for all electrochemical experiments. To avoid contamination of the solution by chloride ions, the reference electrode was in contact with the working electrode through an electrolyte bridge. The Luggin capillary filled with the test solution had a porous ceramic membrane at the end to further delay diffusion of species in the solution. The Luggin capillary tip was placed very close to the electrode surface to minimize the ohmic drop of the solution. Saline solution was freshly prepared from distilled water and pure grade chemicals. The electrolyte was exchanged after each measurement in order to avoid contamination of soluble species. Potentiodynamic measurements were carried out by sweeping the potential in the positive or negative direction with a sweep rate of 1 mV/s until a current limit in the mA range is reached.

Model corrosion tests for 1, 2, 3, 4, 8 days in a 5-% NaCl solution at 293±2 K were carried out with specimens 3.0×0.5 cm in size. The specimens were fully immersed in the saline solution. Testing under these conditions was assumed to be equivalent to a 5-years application in marine atmosphere. The surface morphology was examined using a scanning electron microscope (SEM).

RESULTS AND DISCUSSION

The results of metallographic and XRD analyses of the $Al_{69}Co_{21}Ni_{10}$ alloy are summarized in Fig. 1. Two ternary compounds are found in the structure: the crystalline $Al_9(Co,Ni)_2$ phase and decagonal quasicrystalline (D) phase with the composition $Al_{72}Co_{9.5}Ni_{18.5}$, as EDS measurements show. As the D-phase is observed at room temperature the stability of this phase with respect to decomposition into its neighboring phases is clearly confirmed. The average volume fraction of D-quasicrystals is about 59 vol.% of the total alloy volume [24]. Their sizes range from 50 to 80 μm.

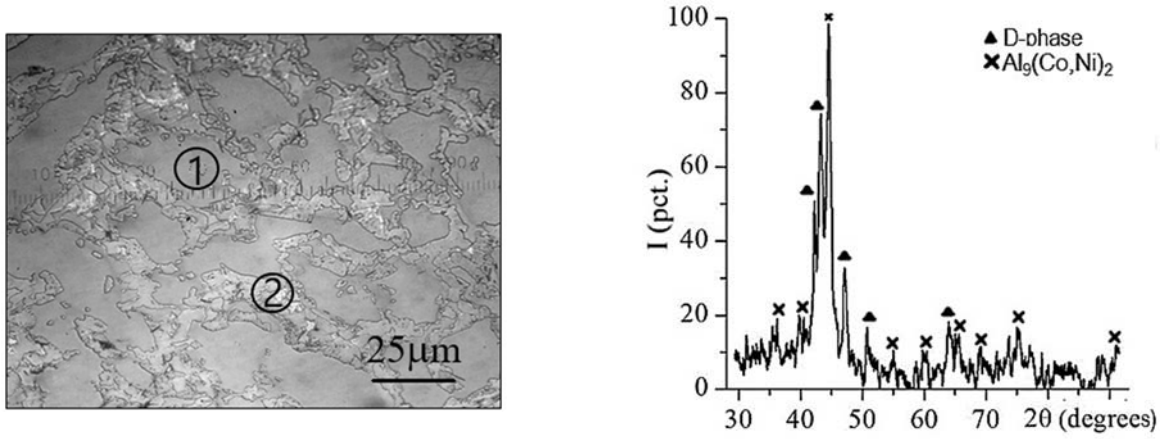

a b

Figure 1. The $Al_{69}Co_{21}Ni_{10}$ alloy: a – OM image, where D-phase (1) and $Al_9(Co,Ni)_2$ (2); b – XRD pattern

The $Al_{72}Fe_{15}Ni_{13}$ alloy exhibits two-phase structure (Fig. 2a). From the XRD, the cast alloy consists of primary Al_5FeNi crystals separated by secondary quasicrystalline decagonal D-phase (Fig. 2b). The estimation of D-phase composition by EDS method gives $Al_{72.5}Ni_{17}Fe_{10.5}$. The volume fraction of D-phase reaches 30 vol. % of a total alloy volume [25].

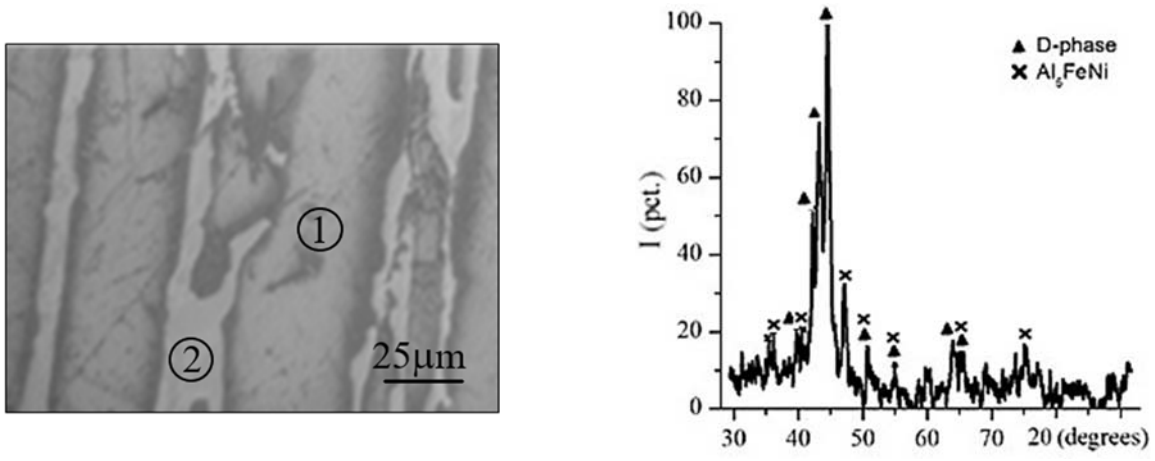

a b

Figure 2. The $Al_{72}Fe_{15}Ni_{13}$ alloy: a – OM image, where Al_5FeNi (1) and D-phase (2); b – XRD pattern

Measurements show that the decagonal D-quasicrystals of $Al_{69}Co_{21}Ni_{10}$ and $Al_{72}Fe_{15}Ni_{13}$ alloys possess a Vickers hardness of about 8.6–10.1 GPa, which is much higher than that for coexisting crystalline phases. Comparison with the intermetallic compounds in the investigated alloys exhibits the following sequence: H(D-AlCoNi)>H(D-AlFeNi)>H(Al_5FeNi)>H($Al_9(Co,Ni)_2$).

The studied alloys do not noticeably corrode in 5-% aqueous NaCl solution. Their color and mass do not essentially change. Due to presence of aluminum, both the $Al_{69}Co_{21}Ni_{10}$ and $Al_{72}Fe_{15}Ni_{13}$ alloys exposed to atmosphere after polishing are spontaneously covered with an oxide film. This thin surface film consists predominately of aluminum oxides with also a small contribution of iron, cobalt or nickel oxides. As soon as samples are immersed in 5-% NaCl solution of pH 7.0, the process of the oxide layer stabilization begins. Fig. 3 shows the change of stationary potentials (E_{st}) of $Al_{69}Co_{21}Ni_{10}$ and $Al_{72}Fe_{15}Ni_{13}$ alloys during 45 min. The recorded results reveal that the stationary potentials of the alloys increase very fast towards more positive values during first 300–500 seconds indicating that the major changes in the passive film occur during this time. Afterwards the potential stabilizes reaching a steady value. The result could be attributed to the stabilization of passive oxide film. The stationary potentials amount to –0.48 V and –0.40 V for $Al_{72}Fe_{15}Ni_{13}$ and $Al_{69}Co_{21}Ni_{10}$ alloy, respectively. The $Al_{69}Co_{21}Ni_{10}$ alloy has a slightly nobler potential which indicates more passive state of its surface.

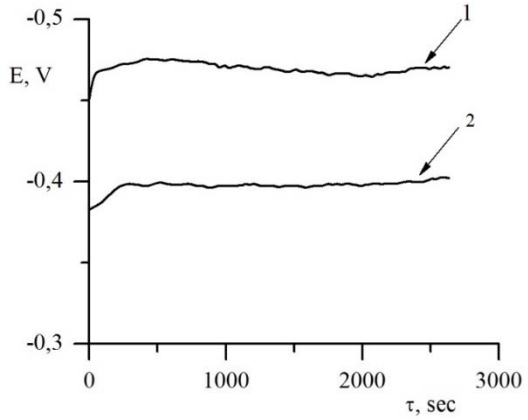

Figure 3. (E,τ)-curves recorded in 5-% NaCl solution (pH=7.0) for $Al_{72}Fe_{15}Ni_{13}$ (1) and $Al_{69}Co_{21}Ni_{10}$ (2) alloys

Fig. 4 illustrates the voltammograms recorded for the $Al_{72}Fe_{15}Ni_{13}$ and $Al_{69}Co_{21}Ni_{10}$ alloys by cyclic potentiodynamic polarization method with periodic sweeping the potential in the opposite directions. As the potential is changed from E_{st} towards more positive values, the anodic current density rises gradually. At potential of ~(–0.3) V, a sharp increase in anodic current is observed which may relate to active dissolution of alloys components. When direction of potential sweep is switched back, the null value of current density is reached at potential of (–0.88) V for the $Al_{72}Fe_{15}Ni_{13}$ alloy (Fig. 4a) and (–0.86) V for the $Al_{69}Co_{21}Ni_{10}$ alloy (Fig. 4b). At potentials more negative than (–1.0) V, a cathodic current density increases which indicates that depolarizer restoration begins. At the next cycle of a potential sweep, the electrochemical passivity regions may be determined. They have close sizes from –1.0 V to –0.5 V for the $Al_{72}Fe_{15}Ni_{13}$ alloy and from –1.0 V to –0.4 V for the $Al_{69}Co_{21}Ni_{10}$ alloy. No active dissolution region is observed, thus indicating that the surface of the alloys is covered with passive oxide layer. This may be explained by the transition of the alloys to passive state due to cobalt and/or nickel present in their composition.

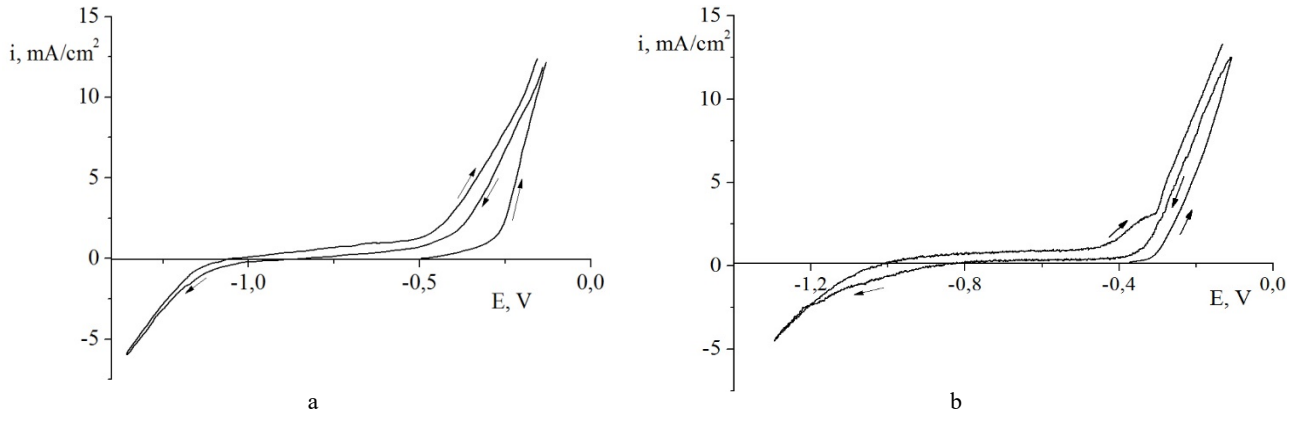

Figure 4. Cyclic voltammogram showing both a positive- and negative-going sweep obtained in 5-% NaCl solution (pH=6.9) for the alloys: a – $Al_{72}Fe_{15}Ni_{13}$; b – $Al_{69}Co_{21}Ni_{10}$.

For both alloys, corrosion in the neutral sodium chloride solution proceeds with oxygen depolarization which gives rise to the close values of the passivity region limit in the negative area of potentials. The extension of electrochemical passivity region towards more positive value of potential for the $Al_{69}Co_{21}Ni_{10}$ alloy may relate to the inhibition of anodic processes. Therefore, the $Al_{72}Fe_{15}Ni_{13}$ alloy has a slightly larger tendency to corrode although the stationary potentials for the investigated alloys follow a similar trend. The (E,lgi)-curves recorded in 5-% NaCl solution are shown in Fig. 5. The intersection point of two plot branches corresponds to a logarithm of corrosion current density (i_{corr}). The value of i_{corr} determined for the $Al_{72}Fe_{15}Ni_{13}$ alloy equals to 0.14 mA/cm^2 (Fig. 5a), and that for the $Al_{69}Co_{21}Ni_{10}$ alloy is 0.12 mA/cm^2 (Fig. 5b).

Analysis of the solution left after electrochemical corrosion of the $Al_{69}Co_{21}Ni_{10}$ and $Al_{72}Fe_{15}Ni_{13}$ alloys in the saline media reveals very little Co and/or Ni in solution, implying that the remaining solid surface would be Co- and/or Ni-rich. Hence, the general trend seems to be that the noblest metals remain at the surface during corrosion, while the other components, such as Fe and/or Al, dissolve.

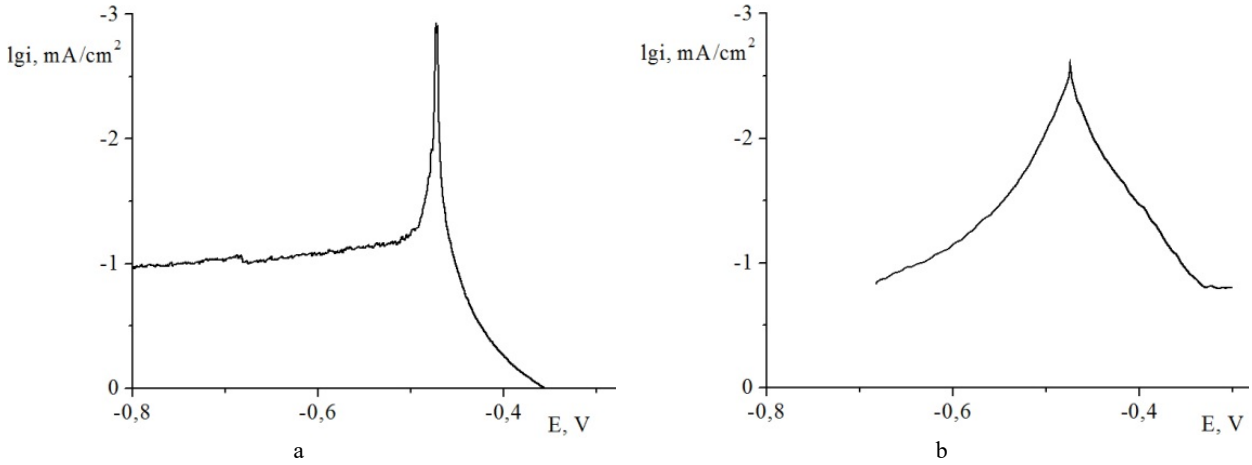

Figure 5. (E,lgi)-curves recorded in 5-% NaCl solution (pH=7.0) for $Al_{72}Fe_{15}Ni_{13}$ (a) and $Al_{69}Co_{21}Ni_{10}$ (b) alloys

After the 8-day immersion test in 5-% NaCl solution, small pits are observed on the surface of the $Al_{72}Fe_{15}Ni_{13}$ alloy (Fig. 6). Pits sites, sized from 5 to 20 μm, are non-uniformly distributed on the surface. The crystalline Al_5FeNi phase and boundaries between the D-phase and Al_5FeNi phase are preferentially dissolved. On the surface of $Al_{69}Co_{21}Ni_{10}$ alloy, pits about 10 μm in size located mainly in the vicinity of defects are revealed as well (Fig. 7). In addition to pitting, preferential dissolution of the interphase boundaries also occurs.

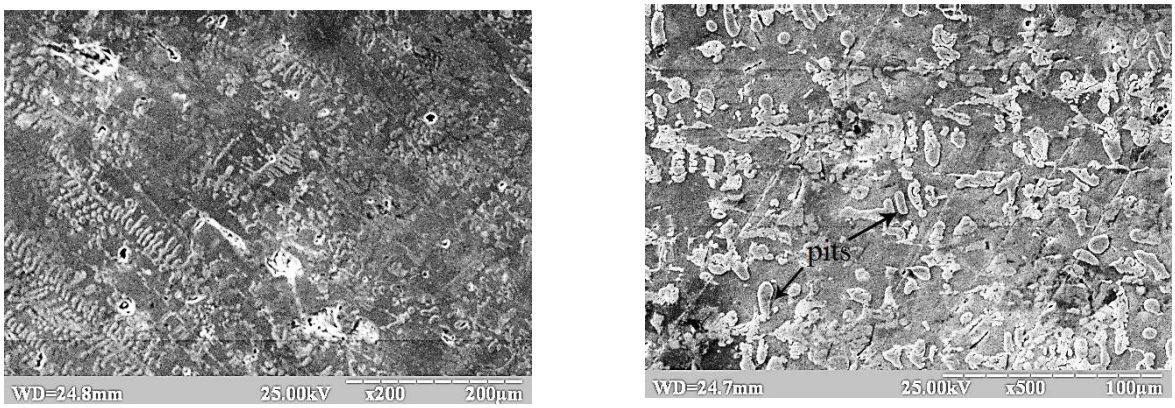

Figure 6. SEM-images of the surface of $Al_{72}Fe_{15}Ni_{13}$ alloy after 8-day immersion test in 5-% NaCl solution (pH=7.0).

Thus, from the electrochemical point of view, the $Al_{69}Co_{21}Ni_{10}$ and $Al_{72}Fe_{15}Ni_{13}$ alloys behave quite similarly in the aqueous sodium chloride solution, but immersion tests show that on the surface of $Al_{72}Fe_{15}Ni_{13}$ alloy visually more pits appear. So, a first order assessment would suggest that the $Al_{72}Fe_{15}Ni_{13}$ alloy has lower resistance to pitting than the $Al_{69}Co_{21}Ni_{10}$ alloy. The reason is that iron-rich phases and their boundaries in the structure of $Al_{72}Fe_{15}Ni_{13}$ alloy are more susceptible to attack by saline solution. The pits on the surface of $Al_{72}Fe_{15}Ni_{13}$ alloy are Ni-rich, apparently forming by dissolution of Al and Fe, and those on the surface of $Al_{69}Co_{21}Ni_{10}$ alloy are Co- and Ni-rich due to preferential dissolution of Al. Corrosion is controlled mainly by chemical composition of the investigated alloys rather than the specific atomic structure of decagonal quasicrystalline D-phase present in their structure.

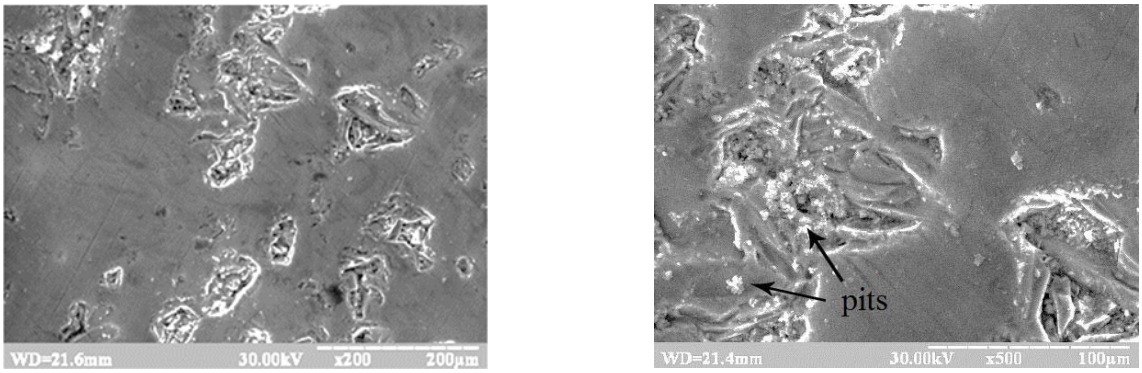

Figure 7. SEM-images of the surface of $Al_{69}Co_{21}Ni_{10}$ alloy after 8-day immersion test in 5-% NaCl solution (pH=7.0).

CONCLUSIONS

The investigations conducted on conventionally solidified $Al_{69}Co_{21}Ni_{10}$ and $Al_{72}Fe_{15}Ni_{13}$ alloys cooled at 5 K/s confirm that both alloys form stable decagonal quasicrystalline D-phase. In $Al_{69}Co_{21}Ni_{10}$ alloy, the primarily solidified phase is D-phase but, in $Al_{72}Fe_{15}Ni_{13}$ alloy, the Al_5FeNi phase. The quasicrystalline D-phase of $Al_{69}Co_{21}Ni_{10}$ alloy coexists with peritectic $Al_9(Co,Ni)_2$ phase. The corrosion of the investigated alloys in 5-% NaCl aqueous solution (pH 6.9-7.0) occurs near the phase boundaries and flawed regions by the electrochemical mechanism. The alloys show an initial stage of dissolution followed by the formation of corrosion layer that blocks further dissolution in the saline solution. The stationary potential for $Al_{69}Co_{21}Ni_{10}$ alloy has more negative value as compared with that for $Al_{72}Fe_{15}Ni_{13}$ alloy. The electrochemical passivity region for $Al_{69}Co_{21}Ni_{10}$ alloy extends due to the inhibition of anodic processes and, therefore, this alloy negligibly corrodes in NaCl solution. As a result, on the surface of the alloy, scarcer and smaller pits are observed. The pits are apparently Ni- or Co-rich, forming by dissolution of Al. The $Al_{72}Fe_{15}Ni_{13}$ alloy has relatively poor corrosion resistance due to preferential dissolution of iron-rich phases in its structure. Therefore, the $Al_{69}Co_{21}Ni_{10}$ alloy shows promise as a coating material to protect rocket-and-space equipment working in marine atmosphere.

The work was performed within the framework of research project No. 0118U003304 “Investigation of the processes of super-rapid quenching from melts and vapor of metal alloys and dielectric compounds“ (2018-2020).

ORCID IDs

Olena V. Sukhova, https://orcid.org/0000-0001-8002-0906; **Volodymyr A. Polonskyy,** http://orcid.org/0000-0002-4810-2626

REFERENCES

[1] K. Edagawa, H. Tamaru, S. Yamaguchi, K. Suzuki, and S. Takeuchi, Phys. Rev. B. **50**, 12413 (1994), https://doi.org/10.1103/PhysRevB.50.1213.
[2] A.-P. Tsai, A. Inoue, and T. Masumoto, Mater. Trans. JIM. **30**(2), 150-154 (1989), https://doi.org/10.2320/matertrans1989.30.150.
[3] L. Zhang, Y. Du, H. Xu, C. Tang, H. Chen, and W. Zhang, J. Alloys Comp. **454**, 129-135 (2008), https://doi.org/10.1016/j.jallcom.2006.12.042.
[4] U. Lemmerz, B. Grushko, C. Freiburg, and M. Jansen, Phil. Mag. Lett. **69**(3), 141-146 (2006), https://doi.org/10.1080/09500839408241583.
[5] B. Grushko and K. Urban, Phil. Mag. B. **70**(5), 1063-1075 (2006), https://doi.org/10.1080/01418639408240273.
[6] B. Grushko and T. Velikanova, Computer Coupling of Phase Diagrams and Thermochemistry. **31**, 217-232 (2007), https://doi.org/10.1016/j.calphad.2006.12.002.
[7] R. Wurschum, T. Troev, and B. Grushko, Phys. Rev. B. **52**(9), 6411-6416 (1995), https://doi.org/10.1103/physrevb.52.6411.
[8] Y. Lei, M. Calvo-Dahlborg, J. Dubois, Z. Hei, P. Weisbecker, and C. Dong, J. Non-Cryst. Solids. **330**, 39-49 (2003), https://doi.org/10.1016/jnoncrysol.2003.08.059.
[9] E. Huttunen-Saarivirta, J. Alloys Comp. **363**(1-2), 150-174 (2004), https://doi.org/10.1016/S0925-8388(03)00445-6.
[10] O.V. Sukhova, V.A. Polonskyy, and K.V. Ustinova, Metallofiz. Noveishie Technol. **40**(11), 1475-1487 (2018), https://doi.org/10.15407/mfint.40.11.1475. (in Ukrainian)
[11] O.V. Sukhova, V.A. Polonskyy, and K.V. Ustinova, Mater. Sci. **55**(2), 285-292 (2019), https://doi.org/10.1007/s11003-019-00302-2.
[12] I.M. Spiridonova, E.V. Sukhovaya, V.F. Butenko, A.P. Zhudra, A.I. Litvinenko, and A.I. Belyi, Powder Metallurgy and Metal Ceramics. **32**(2), 139-141 (1993), https://doi.org/10.1007/BF00560039.
[13] O.V. Sukhova, V.A. Polonskyy, and K.V. Ustinova, Voprosy Khimii i Khimicheskoi Technologii. **6**(121), 77-83 (2018), https://doi.org/10.32434/0321-4095-2018-121-6-77-83. (in Ukrainian)
[14] C. Zhou, R. Cai, S. Gong, and H. Xu, Surf. Coat. Technol. **201**, 1718-1723 (2006), https://doi.org/10.1016/j.surfcoat.2006.02.043.
[15] Y. Kang, C. Zhou, S. Gong, and H. Xu, Mater. Sci. Forum. **475-479**, 3355-3358 (2005), https://doi.org/10.4028/www.scientific.net/MSF.475-479.3355.
[16] D.S. Shaitura and A.A. Enaleeva, Crystallography Reports. **52**(6), 945-952 (2007), https://doi.org/10.1134/S1063774507060041.
[17] S.I. Ryabtsev, V.A. Polonskyy, and O.V. Sukhova, Powder Metallurgy and Metal Ceramics. **58**(9-10), 567-575 (2020), https://doi.org/10.1007/s11106-020-00111-2.

[18] I.M. Spyrydonova, O.V. Sukhova, and G.V. Zinkovskij, Metall. Min. Ind. **4**(4), 2-5 (2012). (in Russian)
[19] O.V. Sukhova, Metallofiz. Noveishie Technol. **31**(7), 1001-1012 (2009). (in Ukrainian)
[20] I.M. Spiridonova, E.V. Sukhovaya, S.B. Pilyaeva, and O.G. Bezrukavaya, Metall. Min. Ind. **3**, 58-61 (2002). (in Russian)
[21] G. Laplanche, A. Joulain, and J. Bonneville, J. Alloys Comp. **493**, 453-460 (2010), https://doi.org/10.1016/j.jallcom.2009.12.124.
[22] O.V. Sukhova and K.V. Ustinova, Functional Materials. **26**(3), 495-506 (2019), https://doi.org/10.15407/fm26.03.495.
[23] O.V. Sukhova and Yu.V. Syrovatko, Metallofiz. Noveishie Technol. **33**(Special Issue), 371-378 (2011). (in Russian)
[24] O.V. Sukhova and Yu.V. Syrovatko, Metallofiz. Noveishie Technol. **41**(9), 1171-1185 (2019), https://doi.org/10.15407/mfint.41.09.1171.
[25] O.V. Sukhova, V.A. Polonskyy, and K.V. Ustinova, Physics and Chemistry of Solid State. **18**(2), 222-227 (2017), https://doi.org/10.15330/pcss.18.2.222-227.

СТРУКТУРА ТА КОРОЗІЯ КВАЗІКРИСТАЛІЧНИХ ЛИТИХ СПЛАВІВ Al–Co–Ni ТА Al–Fe–Ni У ВОДНОМУ РОЗЧИНІ NaCl

Олена В. Сухова, Володимир А. Полонський
Дніпровський національний університет імені Олеся Гончара
49010, Україна, м. Дніпро, просп. Гагаріна, 72

В роботі досліджено структуру і особливості корозії квазікристалічних литих сплавів $Al_{69}Co_{21}Ni_{10}$ і $Al_{72}Fe_{15}Ni_{13}$ в 5 % розчині натрій хлориду (pH 6,9-7,1). Швидкість охолодження сплавів складала 5 К/с. Структуру сплавів вивчали методами кількісної металографії, рентгеноструктурного аналізу, растрової електронної мікроскопії. Корозійні властивості досліджували потенціодинамічним методом. Величини стаціонарних потенціалів визначали шляхом довготривалої реєстрації (E,τ)-залежностей за допомогою потенціостата ПИ-50-1 та програматора ПР-8 з використанням триелектродної комірки. Допоміжним електродом слугував платиновий електрод, електродом порівняння – хлоридсрібний. Проведені дослідження підтверджують утворення квазікристалічної декагональної D-фази в структурі сплавів $Al_{69}Co_{21}Ni_{10}$ і $Al_{72}Fe_{15}Ni_{13}$. У сплаві $Al_{69}Co_{21}Ni_{10}$ за кімнатної температури D-фаза співіснує з кристалічною фазою $Al_9(Co,Ni)_2$, а в сплаві $Al_{72}Fe_{15}Ni_{13}$ – з фазою Al_5FeNi. У порядку зростання мікротвердості ці фази можна розташувати в такій послідовності: H(D-AlCoNi)>H(D-AlFeNi)>H(Al_5FeNi)>H($Al_9(Co,Ni)_2$). У 5 % розчині натрій хлориду досліджені сплави кородують за електрохімічним механізмом з кисневою деполяризацією. Порівняно зі сплавом $Al_{72}Fe_{15}Ni_{13}$, сплав $Al_{69}Co_{21}Ni_{10}$ має менш від'ємні значення стаціонарного електрохімічного потенціалу (–0,48 В і –0,40 В відповідно), а його зона електрохімічної інертності розширюється за рахунок гальмування анодних процесів. Обидва досліджені сплави переходять у пасивний стан у сольовому розчині. Величина струму корозії, розрахована з (E,lgi)–залежностей, для сплаву $Al_{69}Co_{21}Ni_{10}$ складає 0,12 мА/см^2, а для сплаву $Al_{72}Fe_{15}Ni_{13}$ – 0,14 мА/см^2. Після перебування в сольовому розчині на поверхні сплавів виявлені пітінги переважно в місцях розташування міжфазних границь поділу і дефектів. Кількість та розміри пітінгів на поверхні сплаву $Al_{69}Co_{21}Ni_{10}$ значно менші, ніж на поверхні сплаву $Al_{72}Fe_{15}Ni_{13}$. Більш низьку корозійну тривкість сплаву $Al_{72}Fe_{15}Ni_{13}$ пояснено присутністю в його структурі залізовмістних фаз. Послуговуючись отриманими результатами, для створення покриттів на деталях ракетно-космічної техніки, що працюють в умовах морського клімату, рекомендовано сплав $Al_{69}Co_{21}Ni_{10}$.

КЛЮЧОВІ СЛОВА: декагональні квазікристали, структура, мікротвердість, електрохімічна поляризація, пітінгова корозія.

СТРУКТУРА И КОРРОЗИЯ КВАЗИКРИСТАЛЛИЧЕСКИХ ЛИТЫХ СПЛАВОВ Al–Co–Ni И Al–Fe–Ni В ВОДНОМ РАСТВОРЕ NaCl

Елена В. Сухова, Владимир А. Полонский
Днипровский национальный университет имени Олеся Гончара
49010, Украина, г. Днипро, просп. Гагарина, 72

В работе исследовали структуру и особенности коррозии квазикристаллических литых сплавов $Al_{69}Co_{21}Ni_{10}$ и $Al_{72}Fe_{15}Ni_{13}$ в 5 % растворе хлорида натрия (pH 6,9–7,1). Скорость охлаждения сплавов составляла 5 К/с. Структуру сплавов изучали методами количественной металлографии, рентгеноструктурного анализа, растровой электронной микроскопии. Коррозионные свойства исследовали потенциодинамическим методом. Величины стационарных потенциалов определяли путем длительной регистрации (E,τ)–зависимостей с помощью потенциостата ПИ-50-1 и программатора ПР-8 с использованием трехэлектродной ячейки. Вспомогательным электродом служил платиновый электрод, электродом сравнения – хлоридсеребряный. Проведенные исследования подтверждают образование квазикристаллической декагональной D-фазы в структуре сплавов $Al_{69}Co_{21}Ni_{10}$ и $Al_{72}Fe_{15}Ni_{13}$. В сплаве $Al_{69}Co_{21}Ni_{10}$ при комнатной температуре D-фаза сосуществует с кристаллической фазой $Al_9(Co,Ni)_2$, а в сплаве $Al_{72}Fe_{15}Ni_{13}$ – с фазой Al_5FeNi. В порядке увеличения микротвердости эти фазы можно расположить в такой последовательности: H(D-AlCoNi)>H(D-AlFeNi)>H(Al_5FeNi)>H($Al_9(Co,Ni)_2$). В 5 % растворе хлорида натрия исследованные сплавы корродируют по электрохимическому механизму с кислородной деполяризацией. По сравнению со сплавом $Al_{72}Fe_{15}Ni_{13}$, сплав $Al_{69}Co_{21}Ni_{10}$ имеет менее отрицательные значения стационарного потенциала (–0,48 В и –0,40 В соответственно), а его зона электрохимической пассивности расширяется за счет торможения анодных процессов. Оба сплава переходят в пассивное состояние в солевом растворе. Величина тока коррозии, рассчитанная по (E,lgi)–зависимостям, для сплава $Al_{69}Co_{21}Ni_{10}$ составляет 0,12 мА/см^2, а для сплава $Al_{72}Fe_{15}Ni_{13}$ – 0,14 мА/см^2. После пребывания в солевом растворе на поверхности сплавов выявлены питтинги преимущественно в местах расположения межфазных границ и дефектов. На поверхности сплава $Al_{69}Co_{21}Ni_{10}$ питтинги образуются в меньшем количестве и имеют меньшие размеры, чем на поверхности сплава $Al_{72}Fe_{15}Ni_{13}$. Более низкую коррозионную стойкость сплава $Al_{72}Fe_{15}Ni_{13}$ объяснено присутствием в его структуре железосодержащих фаз. С учетом полученных результатов, для создания покрытий на деталях ракетно-космической техники, работающих в условиях морского климата, рекомендован сплав $Al_{69}Co_{21}Ni_{10}$.

КЛЮЧЕВЫЕ СЛОВА: декагональные квазикристаллы, структура, микротвердость, электрохимическая поляризация, питтинговая коррозия.